Optimal design for real-time quantitative monitoring of sand in gas flowline using computational intelligence assisted design framework

Aminu, Kuda Tijjani; McGlinchey, Don; Chen, Yi

Published in:
Journal of Petroleum Science and Engineering

DOI:
10.1016/j.petrol.2019.03.024

Publication date:
2019

Document Version
Author accepted manuscript

Optimal design for real-time quantitative monitoring of sand in gas flowline using computational intelligence assisted design framework

Kuda Tijjani Aminu[a], Don McGlinchey[a] ,Yi Chen[a]

[a]School of Computing, Engineering and Built Environment, Glasgow Caledonian University, Glasgow G4 0BA, UK

Abstract

Global demand for oil and gas is still increasing rapidly. The direct consequence of this is the increased operating pressure amid concerns over increasing sand production. According to the Society of Petroleum Engineers (SPE), 70% of the world's hydrocarbon reserves are contained in reservoirs situated on unconsolidated formations. Given the reality of these formations, sand production will certainly be a problem of significant concern particularly during the later life of the fields when they become more 'mature'. However, to monitor sand and optimise its production for improved recovery and safety, life extension and economy of the fields and ensured reliability, the automatic detection and prediction of sand flow characteristic measurements; sand flow rate (SFR), sand concentration (SC), line pressure drop (PD), and gas velocity (GV), has become an important research topic of great interest. Despite this importance, discussion of the topic is still lacking in the literature. This paper proposes a novel and robust architecture of intelligent real-time sand flow characteristic measurement using an acoustic sensor and computational intelligence assisted design (CIAD) framework. It fully incorporates acoustic signal processing and analysis, prediction algorithms and optimisation algorithms in the design. Acoustic features based on acoustic signal processing techniques are extracted to reduce the dimensionality of the acoustic signals. A classical Artificial Neural Network (ANN) is used to model the non-linear relationships between the acoustic signal characteristics and the flow characteristics measurands. In addition, the ANN algorithm adapts its weights and biases using the Grey Wolf Optimiser (GWO) through minimisation of the cost function during the training phase. Preliminary results obtained on a laboratory test rig demonstrate that an acoustic sensor coupled with CIAD may provide simple and robust practical solution to the measurement problem of particle-laden gas flow characteristics in real-time.

Keywords: Sand production, signal processing, quantitative models, ANN, CIAD, GWO

1 Introduction

Over the years great pressure has been placed on operators within the oil and gas industry globally due to increasing power generation - thus the increase in the popularity of gas and the significant growth in petrochemicals demand [1],[2]. Consequently, regardless of slowing demand in the transport sector, sand production from the hydrocarbon reservoirs is increasing [3]. Sand production in the oil & gas industry is an issue of major concern to the operators as it often results in mechanical wear of equipment thus causing; serious problems to equipment integrity, severe consequences on hydrocarbon production rate and increased safety concerns. It costs the industry millions of dollars each year to mitigate and repair sand production problems including sand disposal and removal [4]. Therefore, effective sand monitoring is a prerequisite for sustainable hydrocarbon production and is particularly important towards minimising operational risks and cost. Traditionally, sand production is minimised with a variety of classical control completion designs which include chemical consolidation [5]–[7], gravel packing [8], Frac Pack [9], wire wrapped/expandable screens [10], metal foam screen [11], selective/oriented perforations [12] or any combination of these techniques.

Nevertheless, all these methods aimed at control to reduce or stop sand production have limitations on hydrocarbon production which are undesirable. For instance, gravel pack designs can reduce the well diameter; the selective perforation completion can impose limitations on production rates. The alternative is to use a platform that can automatically detect and predict sand flow characteristics in the production flowline in real-time so that operators can optimise production, knowing reliably the quantitative information about the sand they are producing. However, to date, there has been no reliable method that can provide such information.

Operators in the industry have now structured an integrated sand management strategy which is a multi-discipline approach targeted to improve production efficiency through continuous sand production optimisation [13]–[16]. It involves exploring knowledge of the reservoir rock strength through characterisation of the geomechanical and petrophysical properties of the geological formation. The key to geomechanical characterisation is to ascertain the change in the formation strength due to reservoir depletion. This is measured by Unconfined Compressive Strength or Thick Wall Cylinder tests [17],[18]. Obviously, when the effective stresses exceed the formation strength due to in-situ stresses related to reservoir depletion, the rock fails and sand production can occur. Following the rock failure, sand prediction models are then developed to provide a prediction for the onset of sand failure and quantitative prediction for a mass of sand that would be produced. These models are evolved from field observation, numerical, analytical and probabilistic assumptions and porosity petro-physical property of the rock is central to their development [16],[19]. The next element of the strategy is the selection of sand control completion designs as a technique for mitigating the production of sand. Particle size distribution analyses from the formation grain sample would be critical in the decision process. However, at the heart of any chosen completion technique is the well-established criteria for operations and optimum production. Moreover, optimum selection also reduces the risk of integrity failure and equipment down time and hence the overall profitability of the project [20]. Also, sand monitoring plays a critical role when seeking to prevent sand production through completion techniques. This specifically allows real-time tracking of sand influx and can be acoustic or erosion based [21],[22]. A combined interaction of all the elements in the strategy enables operators to operate in the region between no and massive sand production.

In recent years, a technique of sand monitoring that is gaining increasing attention within the industry relies on acoustic emission (AE) sensors that are clamped on to the production flowline at the surface [23]–[25]. This is partially because of its non-intrusiveness and partially because of its simplicity of installation. The approach relies on the impingements of the produced sand particles that get transported with the produced hydrocarbon on flow restriction component of the flowline to give a qualitative signature for sand production. The simple assumption is that the sand particles may collide with the pipe wall and such collisions are more often around the flow restriction components where the flow changes direction and that create pressure waves that are captured as acoustic signals by the sensors mounted on the component [26],[27]. The pressure level of the acoustic signal is related to the concentration of the sand particles and hence the trend of sand production. Versatile as the AE technology approach is, the uncertainties of the flow still makes it insufficient for real-time quantitative sand flow characteristics measurement, as that requires certain parameters within the flow system to remain constant which is perhaps a rare scenario [28]. However, one promising method of intelligent sand monitoring that combines the qualitative interpretation capability of the AE technology is automated, real-time sand flow characteristics measurement using CIAD [29]. Thus, the use of advanced signal processing techniques on the acoustic signal generated as the sand particles hit the flowline component coupled with CIAD is considered an opportunity for facilitating real-time quantitative sand flow characteristic measurement in multiphase flowlines such as the particle-laden

gas flowline. Based on the acoustic signal, it is possible to detect and predict the sand flow rate, sand concentration, line pressure drop and gas velocity in the flowline. Developing an automated and robust method would also impact on the predictability and reliability of the flow with consequent economic impact. Recently, techniques for multiphase measurement incorporating traditional sensors and CIAD constituent techniques have been discussed in detail by Yan, *et al*.[30].

Nevertheless, the approach is not a simple task considering the enormous amount of acoustic data believed to carry information on flow characteristics that need to be analysed and that can pose novel technical challenges in real-time applications [31]. In addition, for computational and run time efficiency, it is very uncommon for the prediction algorithms to work directly on the raw acoustic signal. In the sense of this, various informative features are extracted at signal segmental level to establish their relationships with the flow characteristic parameters through the use of the CIAD. Additionally the intended result of the whole process is to transform the raw acoustic signal into a format the CIAD models can easily work with. The trained CIAD models are then used to estimate the flow characteristics parameters. However, different features are available for acoustic signal processing which include zero-crossing rate, energy entropy, spectral flux, spectral centroid, spectral spread, spectral roll-off and spectral entropy [31],[32]. Conventionally, these features are more common in music information retrieval (MIR) and automatic speech recognition (ASR) applications [33], but recently they are used in a wide range of applications including bioacoustics [34], behavioural assessment [35], medical pathology [36] and machine condition monitoring [37].

This paper proposes a novel approach incorporating an acoustic sensor with CIAD framework to construct and optimise a real-time sand flow characteristic measurement solution for particle-laden multiphase flow. The acoustic sensor is employed for its simplicity, non-intrusiveness and low cost. The remaining part of the paper proceeds as follow. Section 2 describes the modelling methods for the proposed CIAD model. Section 3 presents the methodology for the proposed measurement system. Section 4 presents the experimental setup and measurement techniques used in the study. Section 5 provides and discusses the empirical results obtained from the test flow rig. Section 6 concludes the paper.

2 Techniques of modelling; concepts and procedures

2.1 Artificial Neural Network (ANN)

ANNs are computational models inspired by biological neurons and have evolved since the seminal neural model of McCulloch and Pitts [38]. Architecturally, they are made up of highly interconnected units called neurons usually organised in layers and aimed at solving a variety of sophisticated computational problems. This basically consists of an input layer, an output layer and one or more layers between the input and the output often called the hidden layer(s) [39]. The connections between the neurons have weights and biases associated with them and these weights and biases are random at the initial instant. Therefore ANN models are developed by training a network to extract the salient features from the data. In the training phase, input-output relationships are presented to the network and the weights are adjusted iteratively to elicit the correct output more likely. In essence, the ANN is an optimisation process in which a cost function is minimised by adjusting the weights and biases including the other learning parameters. The Backpropagation algorithm (BP) is still one of the most widely used learning algorithms during the training process. It is a gradient-descent based approach commonly employed to minimise the error between the predicted and the actual output. One of the major drawbacks of BP algorithm is convergence to local minima [40]. However, the reality of local

minima is a consequence of the fact that the error curvature is simply the superposition of non-linear activation functions that may exhibit local minima at different locations, which occasionally results in a non-convex curvature of the error cost function [41],[42]. One way to overcome this challenge is through the use of improved gradient-based algorithms that employ parameter adaptation strategies [43]. This can be achieved by the use of global optimisation techniques which can lead to optimal weight adjustments thus allowing the network to eschew local minima during the learning process, and at the same time, selecting the network optimal parameters (learning rate, momentum term and the regularisation term) to realise maximum performance. The implementation of such algorithms in ANN have been presented in the literature like the Simulated Annealing (SA) [44], Genetic Algorithms (GA) [41], Evolutionary Algorithms (EA) [45]. Recently, however, the use of these stochastic optimisation algorithms are highly recommended in hybrid intelligent optimisation systems such as the ANN training due to their high exploratory behaviour [46]. For this reason, the ANN is trained via GWO algorithm, introduced in the next subsection.

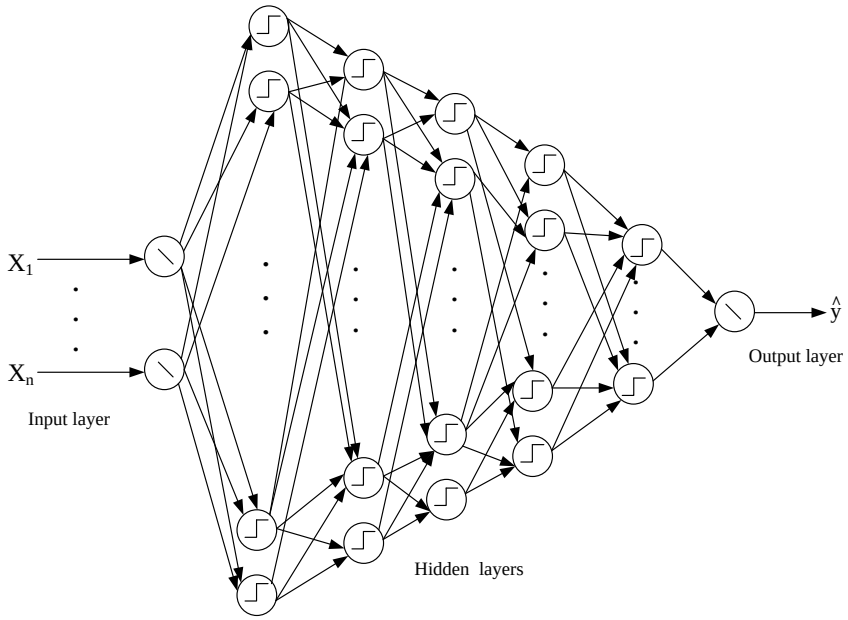

Figure 1. A seven layer ANN model

A seven layer ANN has been modelled due to the complexity of the problem. The seven layer ANN shown in Figure 1 has five hidden layers. In this network, the neurons in the layers of the hidden layer are arranged such that the preceding layer has more neurons than the succeeding layer. This way the complexity of the model increases as the data progresses through the network. The processing neurons in the hidden layers and the output layer have a non-linear activation function using a sigmoid activation function. The architecture of the model is thus $2L$ $25N$ $15N$ $10N$ $5N$ $3N$ $1L$, where L represents linear processing neuron and N indicates non-linear processing neurons. This model is used to capture the distribution of the acoustic feature vector for each output in the training sample.

2.2 GWO algorithm; concepts and principles

GWO is a nature-inspired metaheuristic optimisation algorithm firstly developed by Mirjalili *et al* [47] and mimics the social behaviour of grey wolves in a pack. The algorithm is inspired by the leadership hierarchy and hunting strategy of grey wolves. In order to simulate the leadership hierarchy of wolves for algorithmic development, four types of wolves are considered – the alpha (α), beta (β),

delta (δ) and omega (ω). Moreover, the three hunting strategies of wolves: searching for prey, encircling prey and attacking prey are employed. The next subsections present the algorithm development. The flow chart and the pseudo code for GWO are illustrated in Figure 2.

2.2.1 Leadership hierarchy

Mathematically, GWO is modelled by assuming the best solution to be the alpha. Accordingly, the second and third optimal solutions are regarded beta and delta respectively. The remainder of the prospective solutions are considered to be omega. The optimisation strategy (hunting) in the GWO algorithm is dictated by alpha (α), beta (β) and delta (δ). The omega wolves always submit to the commands of these three wolves [46]–[48].

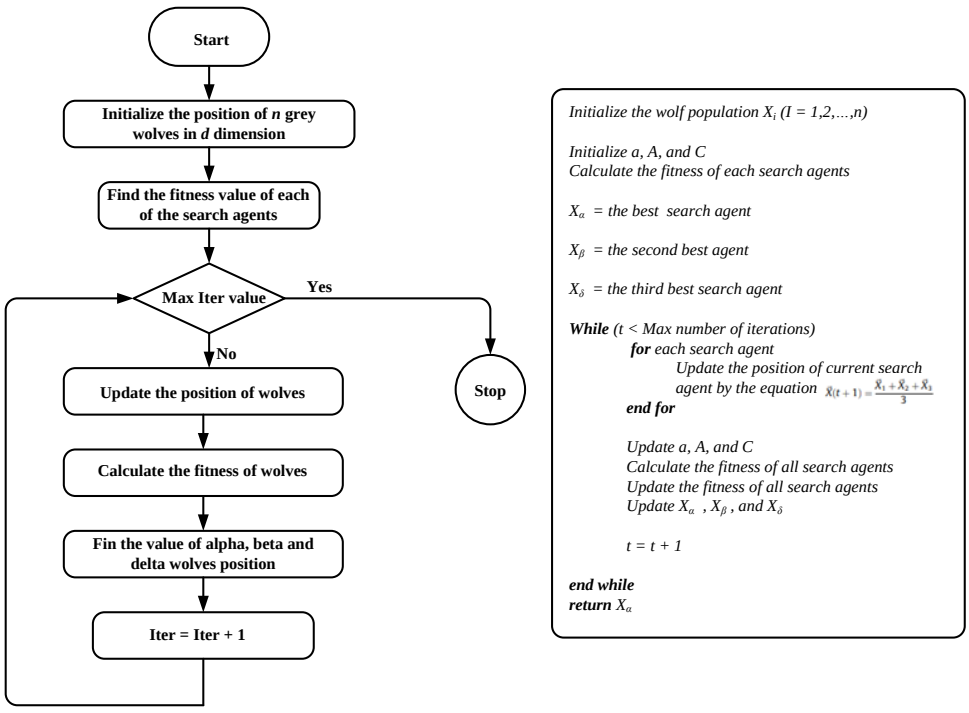

Figure 2. Flow chart (left) and pseudo code (right) of GWO

2.2.2 Encircling prey

As the grey wolves are close to the prey during the hunt, then all the wolves will take position and encircle the prey. The encircling behaviour (distance) can be mathematically represented by the equations:

$$D = \left|CX_p - AX(t)\right| \tag{1}$$

$$X(t+1) = X_p(t) - AD \tag{2}$$

where t represents the current iteration, X is the position vector of a wolf whereas X_p denotes the position vector of the prey , A and C represent the coefficient vectors and D is the encircling behaviour. The vectors A and C are random and adaptive vectors that provide exploration and exploitation for the GWO algorithm and are computed as follows:

$$A = 2\,\vec{a}\;r_1 - \vec{a} \tag{3}$$

$$C = 2r_2 \tag{4}$$

where r_1 and r_2 are random vectors in [0,1] and the components of $\vec{a}$ vary linearly from 2 to 0 over the iteration circle [46]–[48].

2.2.3 Hunting

Grey wolves have an excellent sense of smell which enables them to locate the position of prey, chase and encircle the prey. The hunt is usually guided by the alpha. Occasionally, the beta and delta also take part in the hunt. It is, however, apparent that from the inherent capability of the wolves, the alpha, beta and delta have better knowledge about the prospective location of prey than the omega. Consequently, the first three solutions are considered optimal and the other search agents should update their positions according to the position of the optimal search agents. For this purpose, the following equations are formulated to assume the hunting strategy of the wolves and find the propitious regions for each of the best search agents [46]–[48].

$$D_\alpha = |C_1 X_\alpha(t) - X(t)| \tag{5}$$

$$D_\beta = \left|C_2 X_\beta(t) - X(t)\right| \tag{6}$$

$$D_\delta = |C_3 X_\delta(t) - X(t)| \tag{7}$$

$$X_1 = X_\alpha(t) - A_1(D_\alpha) \tag{8}$$

$$X_2 = X_\beta(t) - A_2\left(D_\beta\right) \tag{9}$$

$$X_3 = X_\delta(t) - A_3(D_\delta) \tag{10}$$

$$X(t+1) = \frac{X_1 + X_2 + X_3}{3} \tag{11}$$

Where t denotes the current iteration, $X_\alpha(t), X_\beta(t)$ and $X_\delta(t)$ indicate the position of the grey wolves α, β and δ at the t^{th} iteration, $X(t)$ denotes the position of the current solution, $C_1, C_2, C_3, A_1, A_2, A_3$ are random vectors. The general steps of the GWO algorithm are presented in Figure (2) (right).

2.3 The conceptual CIAD framework; the combination of ANN and GWO algorithm

This section presents a novel and robust architecture of a prototype real-time flow characteristics measurement in a particle-laden gas flowline. This architecture is illustrated as shown in Figure 3 (left). It is divided into three sections, namely: the data input section; the Computational Intelligence (CI) integrated solver; and the result output section. The data input section prepares the signal data for the CI integrated solver. It pre-processes the acoustic signal data and extracts important acoustic features from the data using signal processing analysis, selects significant features and normalises the features. The main purpose of using signal processing analysis is to segment out the background noise portions and reduce the dimensionality of the acoustic signal. On the other hand, normalisation is a crucial step for the CI integrated solver particularly when solving datasets with features in different ranges. The normalisation used in this work is the min-max normalisation formulated in Equation (12).

$$y = 2\frac{(x - x_{min})}{(x_{max} - x_{min})} - 1 \tag{12}$$

This formula maps x in the interval [-1 1]. In Equation (12), x_{max} is the maximum value of the feature vector and x_{min} is the minimum value of the feature vector. The CI integrated solver is a set of nature-inspired computational algorithms integrated into one solver to estimate or optimise sophisticated real-world problems. This primarily involves one or more of the following approaches: Swarm Intelligence Algorithms (SIA), Fuzzy Logic (FL), Genetic Algorithm (GA), ANN, Simulated Annealing (SA), and Artificial Immune Algorithms (AIA)[49]. In this work, ANN and GWO algorithm are embedded in the solver and the details of these computational approaches are given in sections 2.1 and 2.2. Finally, section C presents the final model from section B that can be integrated into applications for future predictions, (see Figure 3).

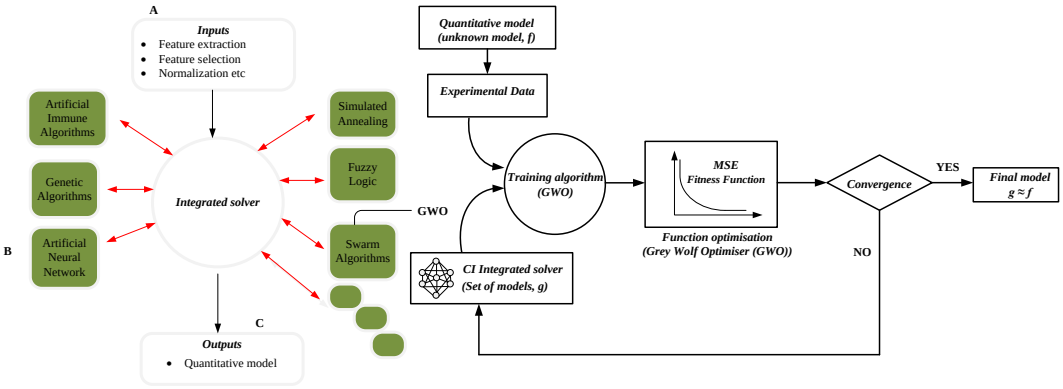

Figure 3. Conceptual framework of computational intelligence assisted design (left) and architecture of the computational intelligence integrated solver (right)

On the CIAD basis, the entire process can be described as depicted in Figure 3(right) in steps as follows. The first step is the target quantitative model which is the ideal magical equation for the estimation and prediction of the sand concentration, sand flow rate, line pressure drop and the gas velocity. Obviously, under this setting, the target models are not readily available. However, what is known about these models is that they are a function from *d*-dimensional acoustic features extracted from signal processing analysis. As a result, this useful information is used as a guide for the construction of successful models for reliable particle-laden flow characteristics prediction. Hence in the next step, there is a dataset of acoustic features – flow characteristics measurement parameter examples obtained from an experiment under controlled conditions. These examples are often referred to as historical data samples. The next step is the learning algorithm that uses the historical data samples to pick a model from a set of models created by the computational intelligence (CI) integrated solver that best approximate the target models. How well the final models approximate the target models is determined by GWO. In addition to overcoming the challenges of the traditional learning algorithm in Backpropagation, the use of the GWO is an attempt to minimise the error measure defined by the sum of squares function using stochastic optimisation (randomisation) and multi-solution based approaches. Thus, adjusting the abstract parameters of the ANN including the weights and biases. The performance of the final models is evaluated based on the average of the sum of squares error function over all the training samples. The final models (trained) are then returned after the satisfaction of the end criterion and used on future acoustic features to estimate flow characteristic measurement parameters.

These abstract parameters of the ANN are defined for the GWO algorithm in the form of a vector as follows:

$$\vec{\Omega} = \{\vec{W}\vec{b}\} = \{W_{1,1}, W_{1,2}, \dots, W_{m,m}, b_1, b_2, \dots b_i\} \tag{13}$$

Where, m represents the number of neurons, $W_{j,i}$ is the weight connection from the j^{th} neuron to the i^{th} neuron, and $b_{j,i}$ corresponds to the bias of the i^{th} hidden neuron. However, given a training dataset, the performance metric is defined by the following mean square error (MSE) function that computes the difference between the target value and the prediction value from the ANN:

$$MSE = \frac{1}{N}\sum_{k=1}^{N}(o_k - d_k) \tag{14}$$

Where, *N* is the number of samples in the training dataset, o_k and d_k respectively represents the target output and the estimated output when the k^{th} training sample is used. It should be noted that d_k is a function of the training samples and the abstract parameters. Since the training samples are fixed, the goal of GWO in training an ANN is to adapt the weights and biases to minimise the MSE function so that the highest possible level of prediction accuracy in sample and out of sample can be obtained. This problem can be formulated with the abstract parameters and the MSE for the GWO algorithm as follows:

$$\min_{(W,b)} F(\vec{\Omega}) = MSE \tag{15}$$

The overall training process of ANN using GWO is depicted in Figure (4). It can be seen from this figure that the GWO algorithm provides ANN with the abstract parameters and receives average MSE for all the samples in the training dataset. Iteratively, the GWO algorithm adjusts these parameters to minimise the average error over whole training samples.

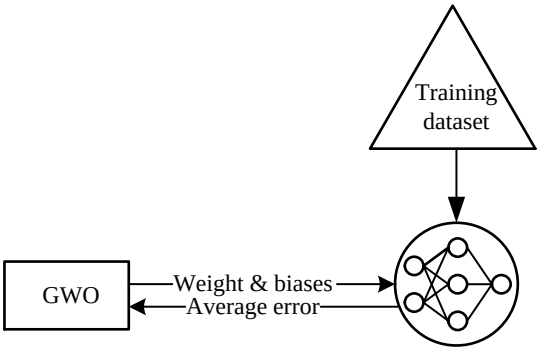

Figure 4. Representative outline of the CIAD framework based on ANN-GWO [46]

3 Methodology

A sketch of the acoustic sensor, location and the entire prototype measurement system is shown in Figure 5. The acoustic sensor was a piezoelectric contact microphone with a diameter of 35 mm and thickness of 0.58 mm. The sensor is mounted externally to a flowline bend where the interactions of the sand particles with the pipe wall is higher and used to capture the sound emitted by the collisions between the particles and the pipe wall. It has a resonance frequency of 40 kHz. The acoustic sensor is

connected to NI – 6212 DAQ device and the resulting signal is digitised with a sampling rate of 44.1 kHz and then processed by the main computer. This hardware has a maximum sampling rate of 400 kS/s and 16-bit digitisation on a single channel. Prior to any signal acquisition, however, the weak acoustic signal is amplified with a voltage gain of 20 dB by the signal conditioning unit. The resulting signal can be transformed using a set of features in time and frequency domains, respectively. This is because time or frequency domain features alone do not provide sufficient description of the signal. These features are presumed to be based on the flow characteristics in the flowline. The relationship between the flow characteristics parameters and the features is highly non-linear and overly complex. For this reason, a CIAD model based on artificial neural network (ANN) and GWO algorithm is determined to represent the underlying functional relationships. For improved computational efficiency and simplified structure of the ANN-GWO model, a neighbourhood component analysis (NCA) is used select the relevant features from the available extracted features that best describe the desired output for the network.

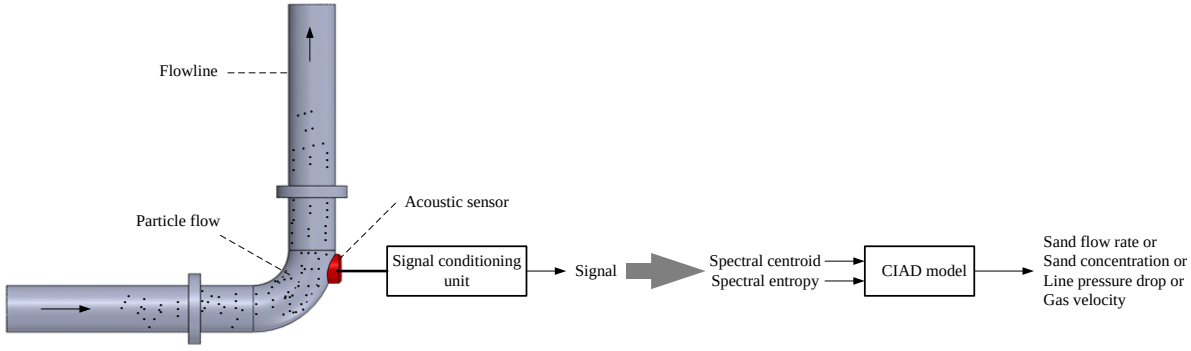

Figure 3. Measurement system based on acoustic sensor and CIAD model

3.1 Signal characteristic features

The flow characteristics of a particle-laden gas flow are a time-varying, dynamic process that can be influenced by flowline conditions and particle characteristics. As a consequence, the signal detected by the acoustic sensor can be considered to have non-stationary characteristics due to the stochastic instinct in the flow. As shown in Figure 6, the original acoustic signal is shaped by a sequence of distinct processes and useful features on the flow characteristics are extracted. A total of twenty six signal features from both time and frequency domains are considered to characterise the signal. Through feature (input) selection using NCA the irrelevant features are eliminated. The inputs of the NCA are the features extracted from the signals and the outputs are weights for each of the features. NCA learns a linear projection of a vector into a space that optimises a criterion related to the leave-one-out accuracy of a nearest neighbour regression model on a training sample [50]. The projection vector, however, defines a Mahalanobis distance metric that can be used by the neighbourhood regression model in the projected space. This method indicates how significant the features are, which gives guidance on how to compose the subset feature vector for building predictive models. The subset of each feature is evaluated by a 5-fold cross validation on the training set. The weights attached for each of the feature indicates what features to use, where a weight above zero implies that the feature is more relevant for predictive model development.

Figure 6. Signal shaping sequence

It was found that the spectral centroid and the spectral entropy have revealed significant correlations with the flow characteristics in the flowline. Therefore, NCA is used to select the most relevant features that contribute significantly to the variations in the data while reducing the dimensionality of the problem. However, a brief description of the selected features is given in the following subsections.

3.1.1 Spectral centroid

The spectral centroid (S_c) of an acoustic signal frequency spectrum reflects the center where most of the energy in the frequency distribution is concentrated. It indicates whether the spectral structure of the signal contains a generality of low or high frequencies, respectively [35],[51]. The spectral centroid of the i^{th} signal frame is computed as seen in Equation (16).

$$S_c(i) = \frac{\sum_{k=0}^{W_{fL}-1} k\,|X_i(k)|}{\sum_{k=0}^{W_{fL}-1} |X_i(k)|} \tag{16}$$

where $X_i(k)$ denotes the magnitude of the discrete Fourier transform (DFT) coefficients, k is the frequency bin for the corresponding coefficient and W_{fL} is the number of coefficients for the signal frame. A large S_c value signifies that the spectrum is dominated by high frequencies whereas a small S_c value indicates that the spectrum is dominated by low frequencies.

3.1.2 Spectral entropy

The spectral entropy (SE) is a feature used to capture the degree of irregularity in the signal spectrum. It is also a measure that relates with the peakiness/flatness of the spectrum [52],[53]. From the computational perspective, the spectrum of the short-term frame is divided into K non-overlapping sub-bands. The spectrum in each of the j^{th} sub-band, $j = 0, \dots, K-1$ is then normalised by the full-band spectrum to obtain the probability function. For the sub-band normalisation, the relation in Equation (17) is utilised [54].

$$s_j = \frac{S_j}{\sum_{j=0}^{K-1} S_j}, \tag{17}$$

being S_j and s_j the energy of the j^{th} sub-band and the probability function (i.e the normalised sub-band spectral energy) respectively. The entropy is then computed using the normalised spectral energy s_j according to the equation:

$$SE(i) = -\sum_{j=0}^{K-1} s_j \log_2(s_j). \tag{18}$$

Nevertheless this sub-division, Equation (18) gives the full-band entropy for the signal frame [54]. Its value is low for a flat frequency distribution and high for a spectrum dominated with sharp peaks.

4 Experimental setup

Experiments were conducted using the Glasgow Caledonian University's multiphase flow test loop facility. The loop has two pressure tanks (sand feeder tank and reception tank) sharing the same air source, controls (PRV and nozzle bank) and has a total flowline length of 12 m and is made of mild steel internal diameter roughly 50 mm. The majority of the flowline sections had horizontal geometry and only about 2.5 m was geometrically vertical. The loop geometry also included five 90 degree oriented bends of standard radius dimensions. The gas required in the loop is supplied at 7.5 barg by two parallel SSR-ML 45 Ingersol Rand screw compressors each with a capacity of 7.4 standard cubic meter per minute through an integrated gas tank. The gas tank is capable of suppressing gas dew point temperature by 11^{o}C. Figure 7 depicts the schematic of the multiphase flow test loop.

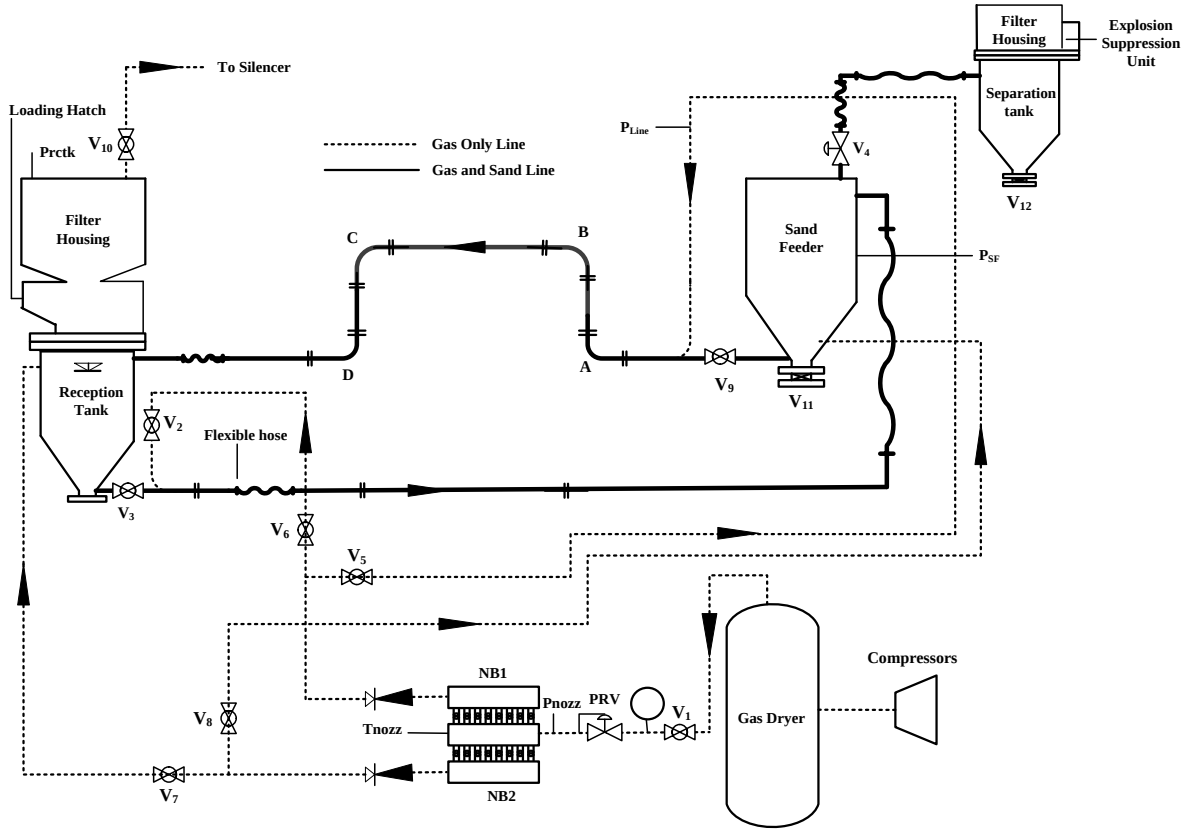

Figure 7. Multiphase flow loop schematic diagram

As shown in Figure 7 the test loop is also equipped with a flow nozzle bank that is used for the control and measurement of gas flow rate. Before the nozzle bank, a pressure control valve (PCV) is used to regulate the amount of gas that enters the nozzle bank. The nozzle bank consists of two rows of nozzles, one row for the transport line (i.e. the top row) and the other for the sand feeder unit (i.e. the bottom row), each of which has 8 nozzles. The total gas flow is determined through a blend of *n* nozzles on the nozzle bank using the formula in Equation (19):

$$\dot{m}_g = \sum_{i}^{n} NN_i \, c_f \, \frac{P_{Upstrean}}{\sqrt{T_{Upstream}}} \; (kg/s) \tag{19}$$

From this equation, NN_i is the nozzle number for each of the nozzles on the nozzle bank and has been estimated experimentally in relation to its cross-sectional area and the discharge coefficient of the nozzle, and c_f is a constant with a value of $0.001K^{1/2}\ m\ s\ Pa/bar$. It should be noted that for all these computations, $P_{Upstream}$ and $T_{Upstream}$ are required to be in absolute units. Invariably, the pressure and temperature sensors are used to monitor the test conditions, particularly the changes in pressure in the upstream, sand feeder, transport line and reception tank. The measuring ranges of the pressure sensors which are all single ended transducers were 0 – 10 bar or 0 – 6 bar. An RTD temperature sensor was installed upstream of the nozzle bank to measure the gas temperature. Sand particles were injected into the flow through the sand feeder. The concentration and velocity of the sand particles were varied by controlling the amount of gas supplied to the system and by varying the proportion supplied to the sand feeder and the transport line. The mass flow rate of the sand particles was measured using load cells. The increase in reception tank mass over time and under stable flow conditions was used to compute this quantity. Through variation of the sand particles' velocity, a wide range of flow conditions in the flowline can be established. The output from the sensor (acoustic) was processed based on the strong assumption that the signal output carries useful information on the flow characteristics parameters. The flow characteristics parameters are calculated as follows:

$$\dot{m}_s = \frac{sand\ mass\ collected\ (kg)}{Time\ (s)}\ (kg/s) \tag{20}$$

$$sand\ conc = \frac{\dot{m}_s}{\dot{m}_g} \tag{21}$$

$$V_{gas} = \frac{\dot{m}_g}{\frac{\left(P_{Transport\ line}+1.01325\ bar\right)}{RT}\cdot A}\ (m/s) \tag{22}$$

$$\Delta P_{Line} = P_{Transport\ line} - P_{Reception\ tank}\ (bar) \tag{23}$$

Where $\dot{m}_s$ denotes the sand particle flow rate, $\dot{m}_g$ denotes the gas mass flow rate, V_{gas} denotes the gas velocity, $P_{Transport\ line}$ denotes the gauge pressure of the transport line, R indicates the gas rate constant, T represents the upstream temperature, A is the cross-sectional area of the flowline, ΔP_{Line} denotes the line pressure drop and $P_{Reception\ tank}$ is the reception tank pressure. These parameters are essentially important in influencing optimum hydrocarbon production through continuous monitoring and subsequent control of flows.

5 Results and discussion

5.1 Experimental traces

Sand particles with diameter ranging from 63 – 2000 μm were used to evaluate the proposed prototype measurement system. A series of experiments was conducted using the multiphase flow test loop facility described in Section 4. Table 1 summarises the physical properties of the test material and the experimental conditions and Table 2 shows the sand concentration (SC) by mass for five different acoustic signals from the database. Figure 8 shows a typical acoustic signal from the impingements of sand particles on the pipe wall of the bend. These SC values are used in the analysis of the features (spectral centroid and spectral entropy) selected through the NCA input selection process. The results of the analyses are illustrated in Figure 9 and 10 respectively.

Table 1. Physical properties of the test solid particles and experimental conditions

Item	Value
Solid particles	Garside 2EW sand
Particle diameter	63 – 2000 μm
Average particle diameter	360 μm
Upstream pressure	2 – 2.5 bar
Upstream temperature	18 - 26 ^{o}C
Gas mass flow rate	0.005 - 0.007 kg/s
Solid mass flow rate	0.20 – 2.59 kg/s

Table 2. Sand concentrations by mass of the acoustic signals from the database

Concentration number	Sand Concentration (SC)
1	43.7
2	35.4
3	28.9
4	11.6
5	3.0

As shown in Figure 8, there are many peaks in the signal due to the dynamics of the particle-laden flow which is determined by the concentration of the sand particles, gas pressure and flow rate. Figure 9 and Figure 10 show the probability density distribution of the mean value of sequences of the selected features (spectral centroid and spectral entropy) extracted from the signal. It can be seen from Figure 9 that the spectral centroid for the SC = 3.0, 11.6 and 43.7 are clearly shown with high values. It seems to imply that the spectrum of the signals for those sand concentrations is inherently dominated by high frequencies. The only unexpected component of the results is the higher spectral centroid value for the SC = 43.7 signal as the high frequency band implies suspension of the sand particles in the medium. Probable reason for this trend could be that the flow mechanism for that sand concentration was in quasi-suspension flow. On one hand the respective values for this statistic are relatively lower for the other signals. However, taking the uncertainty of particle-laden gas flow behaviours into consideration, these findings are therefore significant.

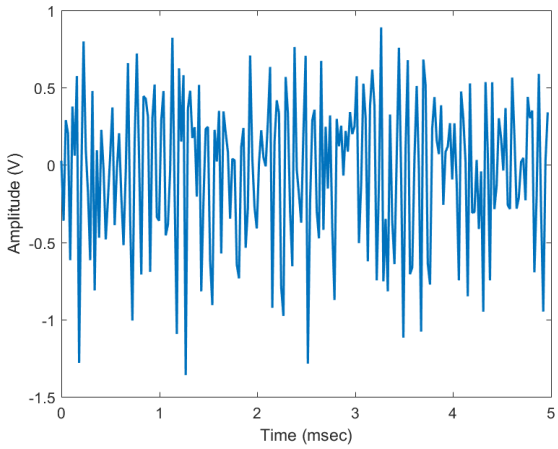

398

399 **Figure 8.** A typical acoustic signal from particles impingements

400

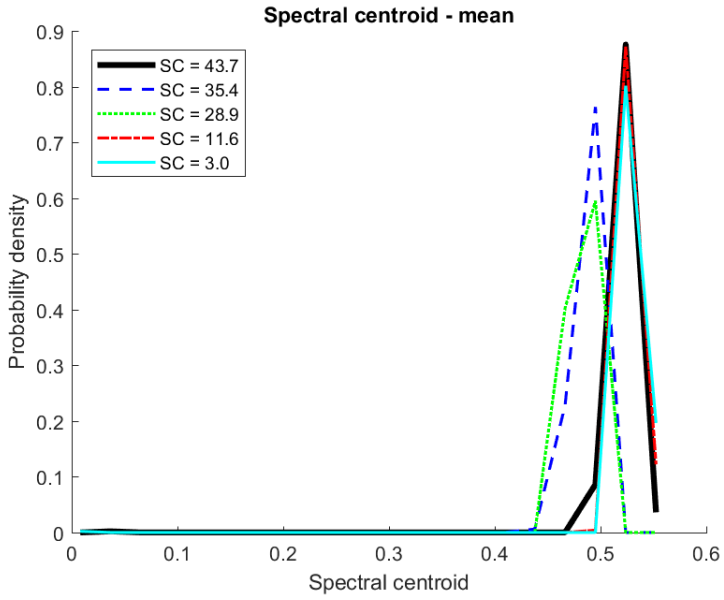

401

402 **Figure 9.** Probability density distribution of the mean of the spectral spread segments of the acoustic
403 signals for different sand concentrations

404 Spectral entropy provides a means to capture the complexity of a signal and uniformity in signal
405 spectrum. Although the results for probability density distribution of the mean of the sequences for
406 spectral entropy segments from the five signals under analysis given in Figure 9 shows the variation
407 of probability density as a function of the spectral entropy values, it is not easy to explain the trends in
408 terms of sand particles interaction with the bend of the flowline. In general, the spectral entropy value
409 is low for a spectrum with flat distribution whereas spectra which contain sharp peaks exhibit higher
410 values. As shown in Figure 10, the SC = 3.0 and SC = 43.7 signal yield the lowest spectral entropy
411 value among the different sand particle concentrations. The reason seems clear: there are irregularities
412 in the distribution of energy in the signal spectra. The values of this statistic for the spectral entropy of
413 SC = 35.4 and SC = 28.9 stay almost identical to that of SC = 11.6 returning a relatively high spectral
414 entropy value and thus implying small variations in the energy distribution. Likewise, the trend for SC

415 = 43.7 and SC = 3.0 but at relatively lower spectral value. Overall, these high values in the spectral
416 entropy indicate the degree of randomness in the spectra of the signals.

417

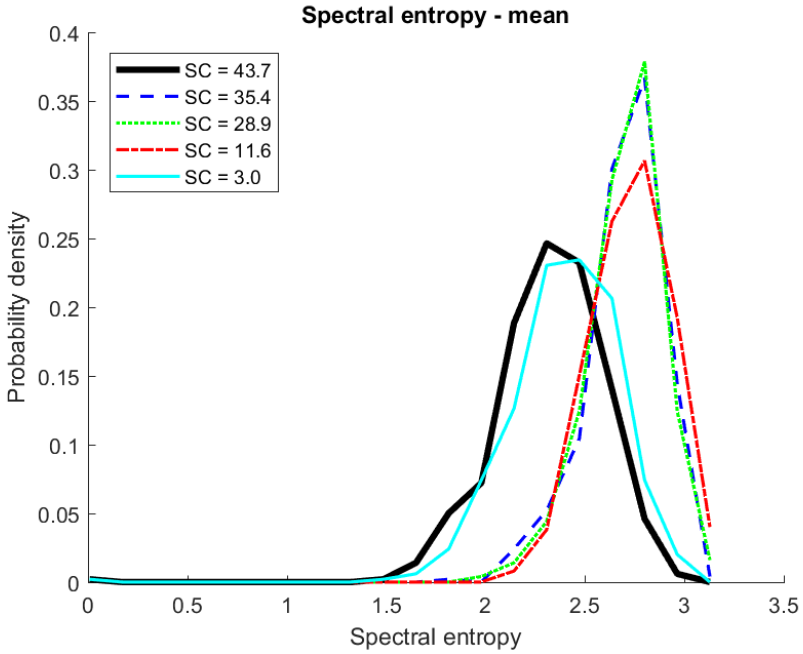

418

419 **Figure 10.** Probability density distribution of the mean of the spectral entropy segments of the
420 acoustic signals for different sand concentrations

421 Figure 11 and Figure 12 show the exploratory analyses of the spectral centroid and the spectral
422 entropy features with the different flow characteristics parameters. The flow characteristics dataset
423 has 2 acoustic features, a total of 800 samples and 4 response parameters (sand flow rate, sand
424 concentration, line pressure drop and gas velocity). Moreover, the total different samples in the
425 dataset were considered in the analyses. In these figures, the flow characteristics parameters were
426 plotted against each of the respective features in an attempt to determine the kind of relationship
427 existing between the variables in the system. As can be seen from these figures, the relationships
428 between the spectral centroid and spectral entropy features with the response parameters are highly
429 non-linear and rather too complex. Mathematically, it is difficult to establish these underlying
430 relationships. However, using the CIAD framework, it can be possible to predict the underlying model
431 and to establish the relationship between the feature parameters and the response parameters. Hence,
432 the CIAD is used to construct and optimise these relationships in this work.

(a)

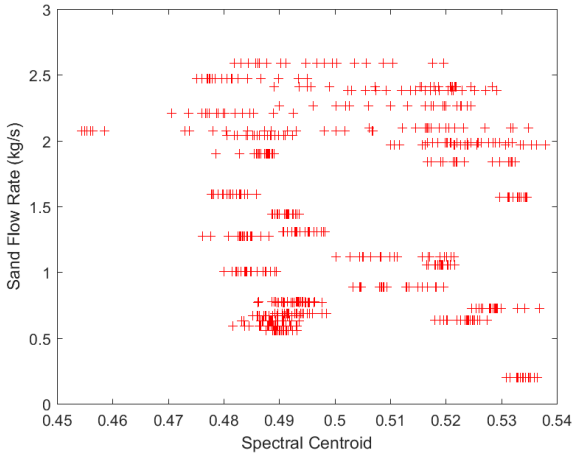

433

(b)

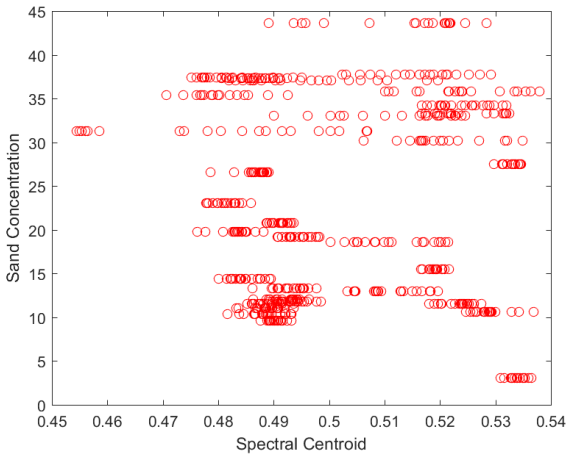

434

(c)

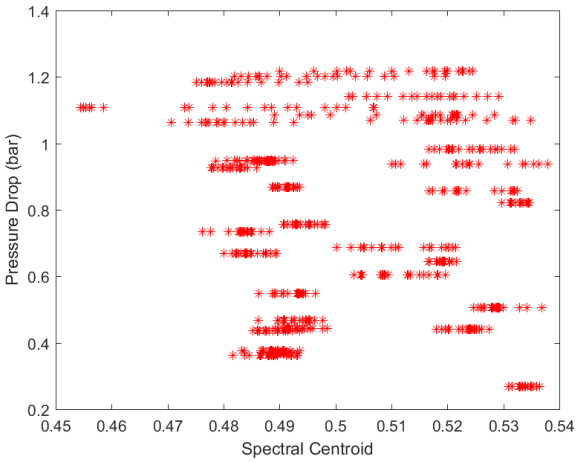

435

(d)

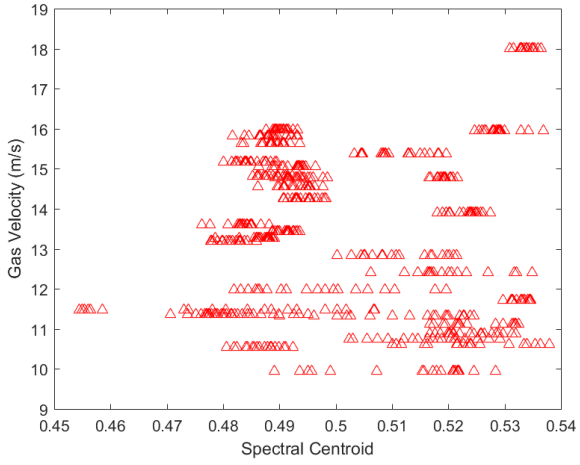

436

437 **Figure 11.** Exploratory analyses of the spectral centroid feature associations with the different
438 response parameters: (a) Sand flow rate (b) Sand concentration (c) Line pressure drop (d) Gas velocity

(a)

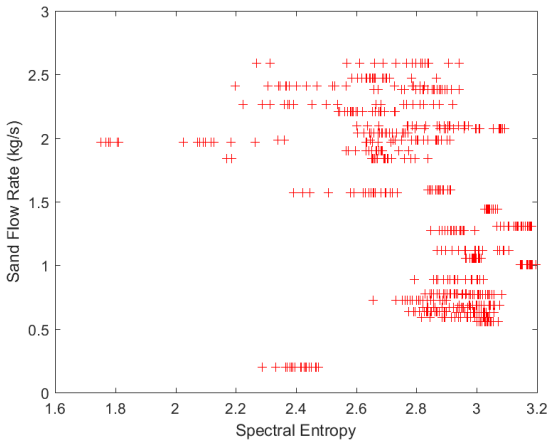

439

(b)

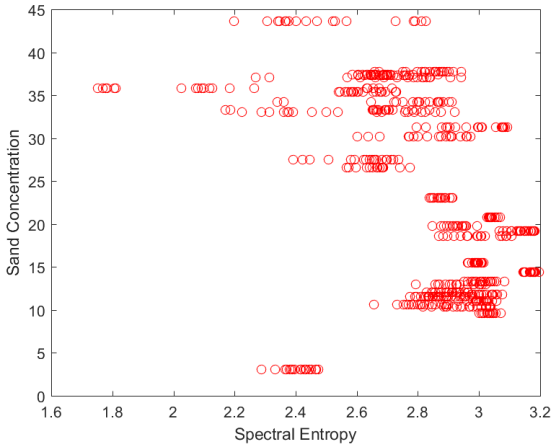

440

(c)

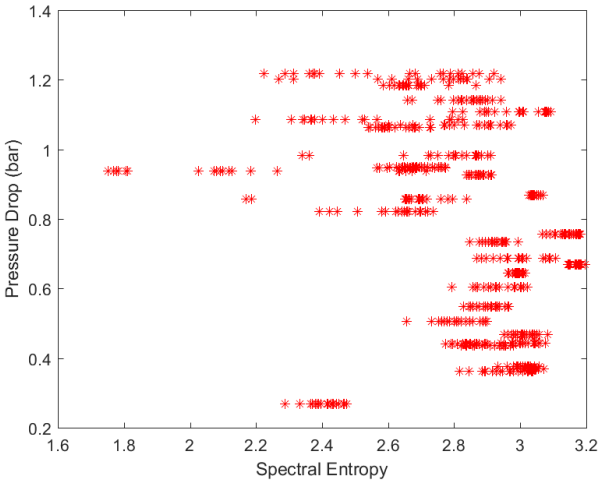

(d)

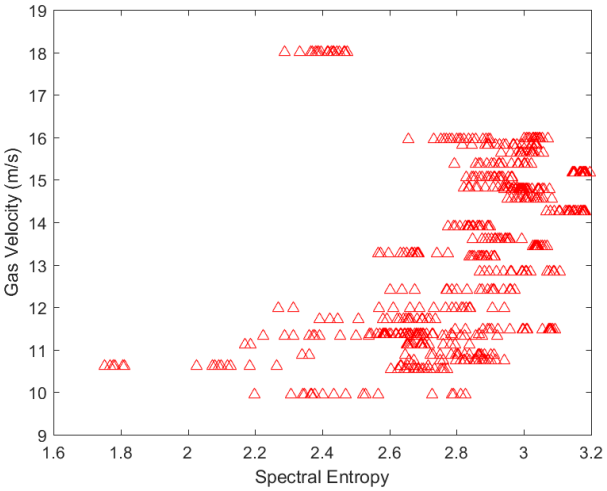

Figure 12. Exploratory analyses of the spectral entropy feature associations with the different response parameters: (a) Sand flow rate (b) Sand concentration (c) Line pressure drop (d) Gas velocity

The total 800 samples were randomly divided and 80% was set aside for training and the remaining for testing. The training samples were used for building the models and the testing samples for testing the performance of the built models. This dataset partitioning is usually acceptable when the dataset is adequately large [46],[55], [56]. The two features extracted from the signals were fed to the ANN-GWO as an input vector. During the training of each of the ANN-GWO network, the desired response for each input vector was the expected values of the corresponding sand flow rate, sand concentration, line pressure drop and gas velocity. As mentioned earlier, GWO optimisation algorithm has been used in training the network and thus facilitating fast convergence and local minima avoidance. In the training process, it is assumed that the GWO optimisation process starts with random values in the range of [-5, 5] for all the abstract parameters. Other assumptions for the GWO and the underlying models for the different response parameters are presented in Table 3.

However, selecting training parameters for an ANN network is an iterative process trying different parameters and evaluating performance. During the network training, after the performance gradient has reached a satisfaction pre-set goal, the training process is terminated. To demonstrate the correlation between the trained CIAD model for each of the flow measurement characteristics

parameters and the predictors (extracted signal features) used in this study, a three-dimensional plot was used as shown in Figure 13, 14, 15 and 16.

Table 3. Ranges for the flow characteristics parameters and initial parameters for GWO

Item	Value
Pressure Drop (PD)	0.27 – 1.22 bar
Sand Flow Rate (SFR)	0.20 – 2.59 kg/s
Gas Velocity (GV)	9.95 – 18.01 m/s
Sand Concentration	3.04 – 43.77
$\vec{a}$	Linearly decrease from 2 - 0
Population size	100
Maximum generation	250

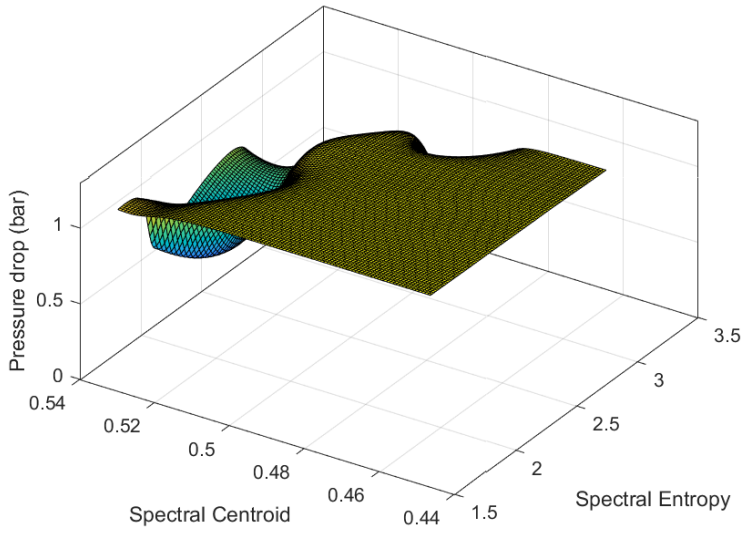

Figure 13. Correlation analysis of pressure drop with spectral centroid and spectral entropy

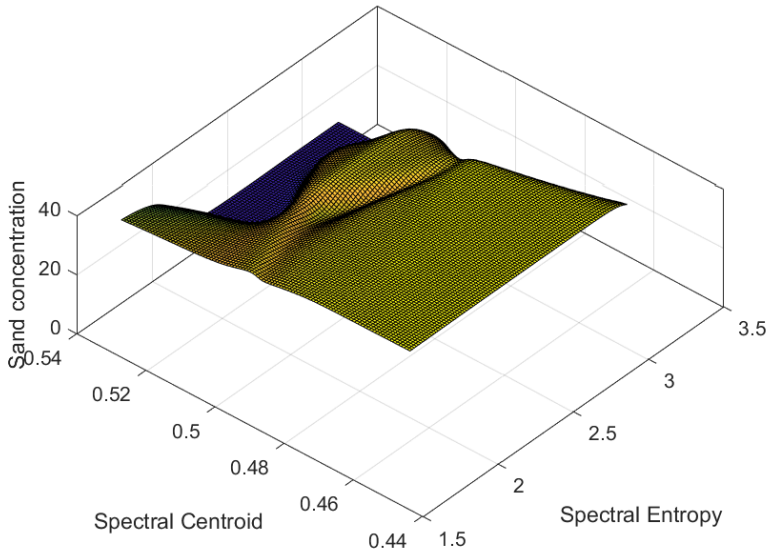

466
467 **Figure 14.** Correlation analysis of sand concentration with spectral centroid and spectral
468 entropy

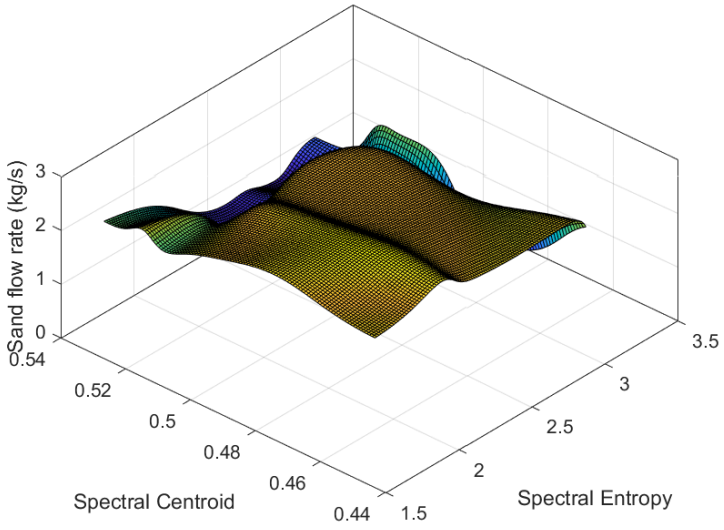

469
470 **Figure 15.** Correlation analysis of sand flow rate with spectral centroid and spectral entropy

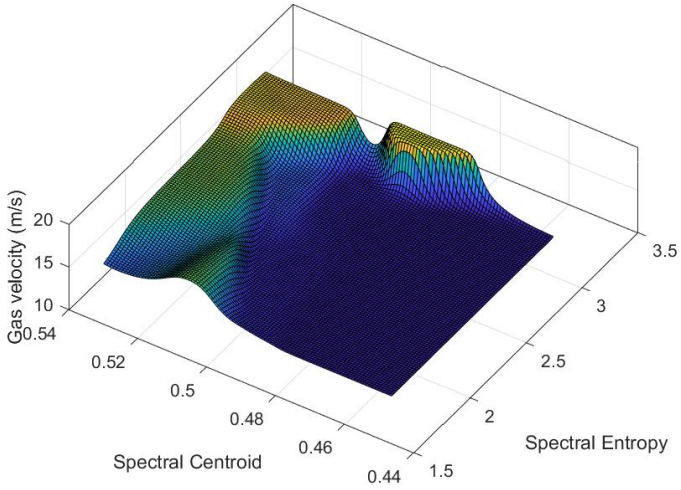

Figure 16. Correlation analysis of gas velocity with spectral centroid and spectral entropy

These figures have further confirmed the non-linear relationships existing between the signal characteristics and the flow characteristics measurands.

5.2 Model performance evaluation

A comparison between the predicted values using the CIAD models and the target value for each of the flow characteristics measurands was done for the testing data. The comparison for SFR, SC, PD and GV CIAD models is presented in Figure 17. The identity line (y = x) is represented by the black solid line in the figure. It is evident from this figure that significant percentage of the predicted values using the CIAD models are close to the actual responses.

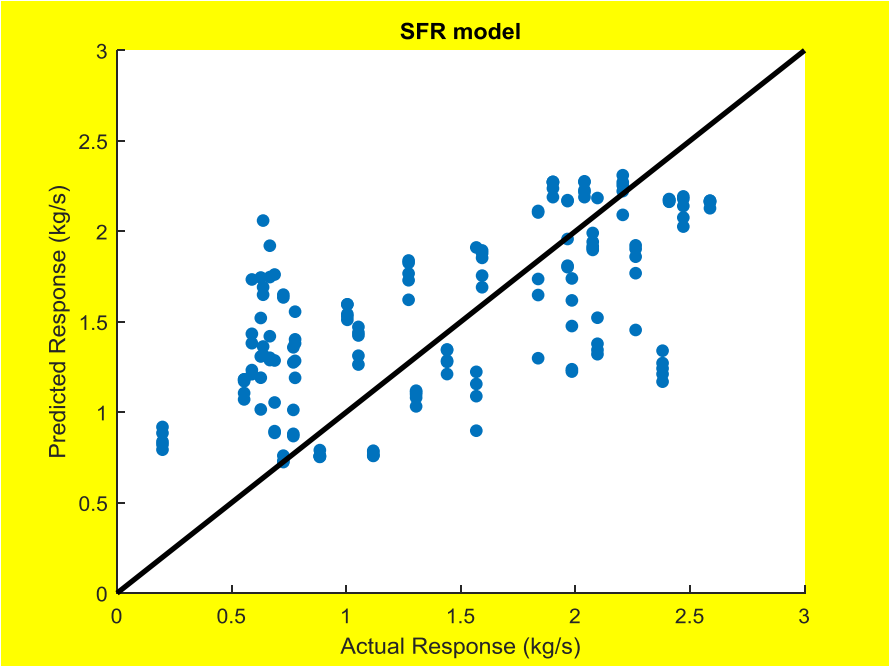

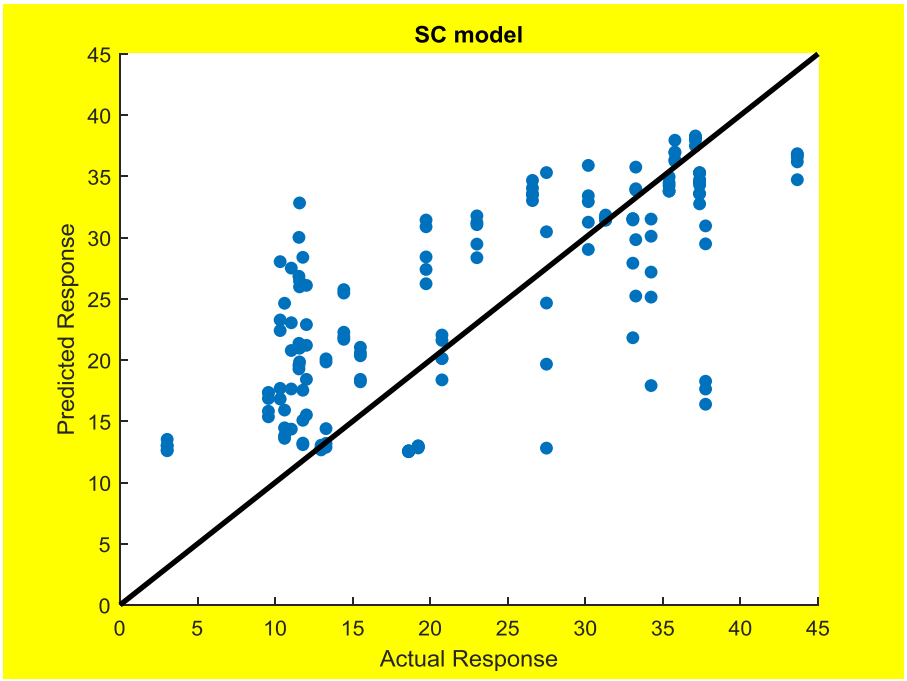
SC model
Predicted Response
Actual Response
0
5
10
15
20
25
30
35
40
45

482

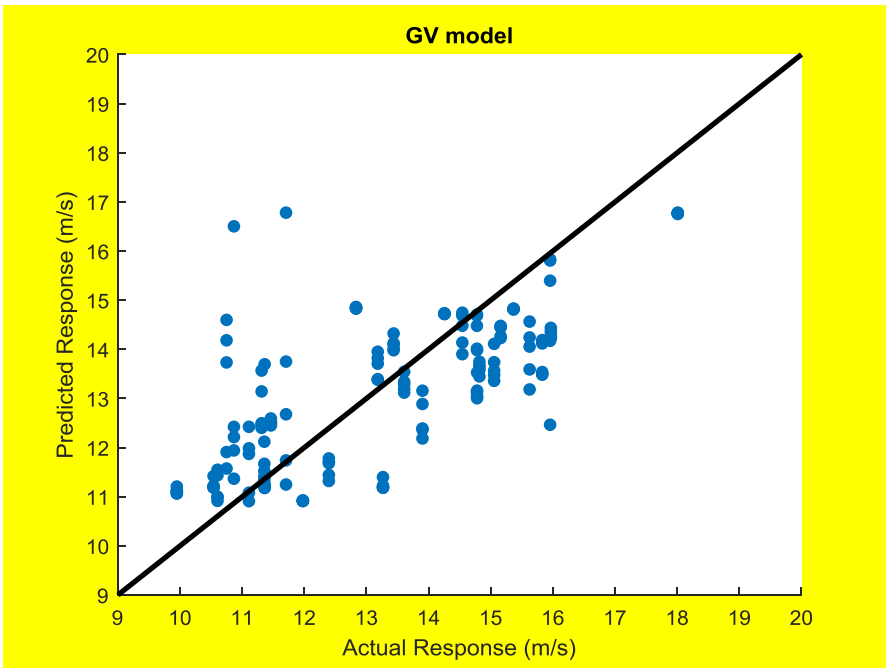
GV model
Predicted Response (m/s)
Actual Response (m/s)
9
10
11
12
13
14
15
16
17
18
19
20

483

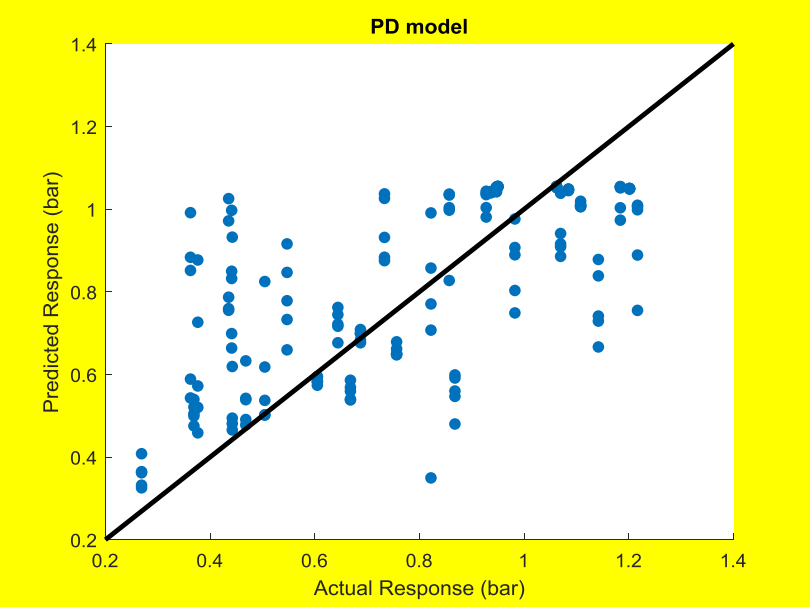

Figure17. Comparisons between the actual target response and the ANN-GWO based CIAD model predicted response of the different measurands

The prediction performances of the proposed CIAD models are evaluated through the correlation factor (R^2), standard deviation (SD), mean absolute error (MAE), maximum absolute error, minimum absolute error, mean absolute relative error (MARE), maximum absolute relative error and minimum absolute relative error. The results of these quantitative error analyses of the suggested CIAD models, in predicting the pressure drop, gas velocity, sand flow rate and sand concentration are presented in Table 5. According to Table 5, in the training samples, MAE and SD (%) for predicting the pressure drop, gas velocity, sand flow rate and sand concentration output are 0.1485 and 3.59 %, 0.9370 and 15.54 %, 0.3525 and 20.48 %, and, 5.0019 and 29.12 % respectively. Also, for the testing samples, these error measures are 0.1612 and 4.51 %, 1.1224 and 20.02 %, 0.4427 and 28.86 %, and, 6.0802 and 34.03 % respectively for pressure drop, gas velocity, sand flow rate and sand concentration output. Furthermore, based on the results presented in Table 5, R^2 values of 0.5886, 0.6169, 0.6039 and 0.6499 for the pressure drop, gas velocity, sand flow rate and sand concentration models respectively, were obtained from the training samples. Likewise, for the testing samples these values are 0.5152, 0.5045, 0.5125 and 0.5221 for the pressure drop, gas velocity, sand flow rate and sand concentration models respectively. Furthermore, it is worth discussing the significance of the R^2 values obtained in this subsection. Though, these values appear not too great, however, they are generally acceptable particularly in situations where the relationship between the input and the output is highly complex and non-linear. This also applies to particle-laden multiphase flow where the flow of particles is considered a time varying and dynamic process. Consequently, the acoustic signal emitted from particles collisions with the flowline can be considered as a random variable and so also are the flow characteristics parameters. Notwithstanding these fairly good performances from the built models, however, the approach is still a step towards providing a much needed cost-effective measurement solution to the long-standing challenge of sand production in the petroleum industry.

513 **Table 5.** Quantitative error analysis of CIAD model accuracy

Statistical parameters	PD model	GV model	SFR model	SC model
Training				
R^2	0.5886	0.6169	0.6039	0.6499
SD (%)	3.59	15.54	20.48	29.12
MAE	0.1485	0.9370	0.3525	5.0019
Maximum absolute error	0.6405	5.0648	1.4910	22.4362
Minimum absolute error	0.0009	0.0025	0.0008	0.0049
MARE (%)	22.82	7.15	39.47	25.45
Maximum absolute relative error	1.9724	0.4327	5.4551	1.2821
Minimum absolute relative error	0.0016	0.0002	0.0010	0.0002
Testing				
R^2	0.5152	0.5045	0.5125	0.5221
SD (%)	4.51	20.02	28.86	34.01
MAE	0.1612	1.1224	0.4427	6.0802
Maximum absolute error	0.6290	5.6356	1.4219	21.3501
Minimum absolute error	0.0021	0.0112	0.0012	0.0834
MARE (%)	26.73	8.62	43.29	45.24
Maximum absolute relative error	1.7351	0.5186	3.6310	3.4522
Minimum absolute relative error	0.0042	0.0009	0.0170	0.0040

514

515 ## 6 Conclusions

516 A novel approach for the measurement of flow characteristics of particle-laden gas flow in a flowline
517 has been presented in this paper using an acoustic sensor and CIAD framework. Performance of the
518 developed models based on CIAD approach, using both quantitative and graphical error analyses. The
519 results from the quantitative error analysis showed that the MAE for predicting the pressure drop, gas
520 velocity, sand flow rate and sand concentration output using the test samples are 0.1485, 0.9370,
521 0.3525, and 5.0019 respectively. The standard deviation of the measurement errors for predicting the
522 pressure drop, gas velocity, sand flow rate and sand concentration output are 3.59 %, 15.54 %, 20.48
523 % and 29.12 % respectively. This performance evaluation suggests that the proposed method is a
524 promising approach to the development of a real-time measurement system.

525 However, substantial further research and development work is required to advance the technology.
526 Firstly, constituent technique of CIAD framework should be explored to model temporal dynamics in
527 the emitted acoustic signal. Secondly, effective denoising techniques should be employed to denoise
528 the signals prior to feature extraction processes. It is envisaged that denoising the signals would help
529 establish greater degree of accuracy in the predicted variables. Thirdly, the practical implementation
530 of the proposed technique on industrial plant conditions should also be conducted to determine its
531 effectiveness. Therefore, a future publication will present performance results in which these
532 recommendations have been implemented. These results will further demonstrate that the proposed
533 approach offers a robust practical solution to meet the difficult quantitative measurement
534 requirements in the petroleum industry.

535 Acknowledgement

536 The authors would like to acknowledge the EPSRC funded ARCHIE-WEST High performance
537 computer from where the results for signal processing were obtained. EPRC grant no. EP/K000586/1.

538 References

539 [1] B. Dudley, “BP Energy Outlook 2017 edition BP Energy Outlook 2017 edition,” 2017.

540 [2] U.S. Energy Information Administration, *International Energy Outlook 2016*, vol. 0484(2016),
541 no. May 2016.

542 [3] C. H. Rawlins, T. J. Hewett, and K. Engineers, “A Comparison of Methodologies for Handling
543 Produced Sand and Solids to Achieve Sustainable Hydrocarbon Production,” *Corrosion*, 2007.

544 [4] S. R. Jackson, B. Gundemoni, and P. Barth, “Sand Control in Corrosive and Erosive
545 Downhole Conditions at High Temperatures,” in *SPE Asia Pacific Oil & Gas Conference and*
546 *Exhibition*, 2016, pp. 1–16.

547 [5] A. I. Othman, S. B. M. Zaki, C. O. E. Pcsb, A. Naharindra, and C. O. E. Pcsb, “Sand
548 Consolidation Case History and Lessons Learned from Peninsular,” in *SPE/ICoTA Coiled*
549 *Tubing & Well Intervention Conference & Exhibition*, 2017, pp. 1–21.

550 [6] P. Fartiyal, A. Tiwari, A. Malik, C. Manickavasagam, N. M. Sharma, and S. Lele, “Effective
551 use of Chemicals to Increase Production in a Mature Asset,” in *SPE Oil and Gas India*
552 *Conference and Exhibition*, 2017, p. 26.

553 [7] S. Mishra and K. Ojha, “A Novel Chemical Composition to Consolidate the Loose Sand
554 Formation in the Oil Field,” in *International Petroleum Technology Conference*, 2016, p. 16.

555 [8] S. Judhan and T. Limited, “An Evaluation of Sand Control Performance within a Field in the
556 Trinmar,” in *SPE Energy Resources Conference*, 2016, p. 15.

557 [9] N. K. Mishra, A. Singh, S. Rakundal, K. W. S. Rajendra, and S. P. Nainwal, “A New
558 Approach for Productivity Enhancement in Mature Sand Prone Fields Having Nearby Water
559 Contact Through Slick Water FracPack : A Case Study,” in *SPE Oil and Gas India Conference*
560 *and Exhibition*, 2017, p. 12.

561 [10] R. Salehi-Moorkani, G. A. Safian, and A. Mirzaei-Paiaman, “Successful applications of
562 expandable sand screen in Persian oil fields, Part 1,” *SPE Prod. Oper. Symp. Proc.*, pp. 1–6,
563 2010.

564 [11] X. Pei, B. Shi, L. Chen, and L. Zheng, “Metal Foam Sand Control Screen,” in *SPE Asia*
565 *Pacific Oil & Gas Conference and Exhibition*, 2013, pp. 1–8.

566 [12] M. Travis, J. Tovar, and J. L. C. Chambers, “Integrated Approach to Sand Control Delivers
567 Zero Sand,” *Proc. SPE Lat. Am. Caribb. Pet. Eng. Conf.*, pp. 282–288, 2003.

568 [13] M. Ruslan *et al.*, “History Case : Integrated Approach to Sand Management and Completion
569 Evaluation for Sand Producer in Mature Field North Sea,” in *SPE Annual Technical*
570 *Conference and Exhibition*, 2016, p. 17.

571 [14] T. Junmano, B. Lee, G. Grant, P. Raipairi, N. Viriyasomboon, and N. Nopsiri, “Sand
572 Production Management the Critical Challenge in Zawtika Gas Production,” in *International*
573 *Petroleum Technology Conference*, 2016, no. 2015, pp. 1–20.

574 [15] A. Gupta *et al.*, “Holistic Sand Management Methodology : A Multi-Disciplinary Team
575 Approach to Cater Sub-Surface & Surface Aspects of Sand Production and,” in *Offshore*
576 *Technology Conference*, 2016, p. 13.

577 [16] M. B. Oyeneyin, “Total Sand Management Solution For Guaranteed Flow Assurance In,” in
578 *SPE Annual International Conference and Exhibition*, 2014, vol. 172429–MS, pp. 1–22.

[17] B. Wu *et al.*, "A New and Practical Model for Amount and Rate of Sand Production," in *Offshore Technology Conference*, 2016, p. 18.

[18] C. A. Mcphee, Z. R. Lemanczyk, P. Helderle, D. Thatchaichawalit, and N. Gongsakdi, "Sand Management in Bongkot Field, Gulf of Thailand: An Integrated Approach," in *SPE Asia Pacific Oil & Gas Conference and Exhibition*, 2000, vol. 64467, pp. 1–10.

[19] H. Wang and M. M. Sharma, "The Role of Elasto-Plasticity in Cavity Shape and Sand Production in Oil and Gas Wells," in *SPE Annual Technical Conference and Exhibition*, 2017, p. 14.

[20] S. Maclachlan, C. S. Harper, B. Hughes, and R. Development, "A Holistic Approach to Sand Control," in *SPE Bergen Seminar*, 2016, pp. 1–10.

[21] M. Odigie, S. A. Shirazi, B. S. McLaury, and S. Cremaschi, "Acoustic Monitor Threshold Limits for Sand Detection in Multiphase Flow Production System," *SPE Int. Conf. Exhib. Oilf. Corros.*, vol. 154378, pp. 1–13, 2012.

[22] A. Nabipour, B. Evans, M. Sarmadivaleh, and C. Kalli, "Methods for Measurement of Solid Particles in Hydrocarbon Flow Streams," *SPE Asia Pacific Oil Gas Conf. Exhib.*, no. 158580, pp. 1–14, 2012.

[23] A. Gupta *et al.*, "Getting the Best Out of Online Acoustic Sand Monitoring System : A Practical Method for Quantitative Interpretation," in *International Petroleum Technology Conference*, 2016, pp. 1–11.

[24] P. Thiruvenkatanathan, T. Langnes, P. Beaumont, D. White, and M. Webster, "Downhole Sand Ingress Detection Using Fibre-Optic Distributed Acoustic Sensors," in *International Petroleum Exhibition & Conference*, 2016, p. 9.

[25] M. E. El-Alej, "Monitoring Sand Particle Concentration in Multiphase Flow Using Acoustic Emission Technology," *World Acad. Sci. Eng. Technol.*, vol. 7, no. 6, pp. 1–7, 2014.

[26] D. Sun *et al.*, "On-line nonintrusive detection of wood pellets in pneumatic conveying pipelines using vibration and acoustic sensors," *IEEE Trans. Instrum. Meas.*, vol. 63, no. 5, pp. 993–1001, 2014.

[27] D. Sun, Y. Yan, R. M. Carter, G. Lu, G. Riley, and M. Wood, "Detecting the Presence of Large Biomass Particles in Pneumatic Conveying Pipelines Using an Acoustic Sensor," pp. 3–6.

[28] A. Mackinnon, J. Brown, and G. K. Brown, "Keeping Acoustic Sand Monitoring Simple," *Corros. Conf. Expo*, no. 11396, pp. 1–14, 2011.

[29] Y. Chen and Y. Li, *Computational Intelligence Assisted Design: In Industrial Revolution 4.0*. CRC Press, 2018.

[30] Y. Yan, L. Wang, T. Wang, X. Wang, Y. Hu, and Q. Duan, "Application of soft computing techniques to multiphase flow measurement : A review," *Flow Meas. Instrum.*, vol. 60, no. November 2017, pp. 30–43, 2018.

[31] D. Mitrović, M. Zeppelzauer, and C. Breiteneder, "Features for Content-Based Audio Retrieval," in *Advances in Computers*, vol. 78, no. 10, 2010, pp. 71–150.

[32] T. Giannakopoulos, *Introduction to AUDIO ANALYSIS : A MATLAB Approach*. 2014.

[33] S. A. Majeed, H. Husain, S. A. Samad, and T. F. Idbeaa, "Mel frequency cepstral coefficients (Mfcc) feature extraction enhancement in the application of speech recognition: A comparison

study," *J. Theor. Appl. Inf. Technol.*, vol. 79, no. 1, pp. 38–56, 2015.

[34] J. Xie, M. Towsey, J. Zhang, and P. Roe, "Acoustic classification of Australian frogs based on enhanced features and machine learning algorithms," *Appl. Acoust.*, vol. 113, pp. 193–201, 2016.

[35] P. N. Le, E. Ambikairajah, J. Epps, V. Sethu, and E. H. C. Choi, "Investigation of spectral centroid features for cognitive load classification," *Speech Commun.*, vol. 53, no. 4, pp. 540–551, 2011.

[36] G. Muhammad and M. Melhem, "Pathological voice detection and binary classification using MPEG-7 audio features," *Biomed. Signal Process. Control*, vol. 11, no. 1, pp. 1–9, 2014.

[37] I. Ubhayaratne, M. P. Pereira, Y. Xiang, and B. F. Rolfe, "Audio signal analysis for tool wear monitoring in sheet metal stamping," *Mech. Syst. Signal Process.*, vol. 85, no. February 2016, pp. 809–826, 2017.

[38] W. S. McCulloch and W. Pitts, "A logical calculus of the ideas immanent in nervous activity," *Bull. Math. Biophys.*, vol. 5, no. 4, pp. 115–133, 1943.

[39] M. Riedmiller, "Advanced supervised learning in multi-layer perceptrons—from backpropagation to adaptive learning algorithms," *Comput. Stand. Interfaces*, vol. 16, no. 3, pp. 265–278, 1994.

[40] A. D. Anastasiadis, G. D. Magoulas, and M. N. Vrahatis, "Sign-based learning schemes for pattern classification," *Pattern Recognit. Lett.*, vol. 26, no. 12, pp. 1926–1936, 2005.

[41] V. P. Plagianakos, G. D. Magoulas, and M. N. Vrahatis, "Learning in multilayer perceptrons using global optimization strategies," *Nonlinear Anal. Theory, Methods Appl.*, vol. 47, no. 5, pp. 3431–3436, 2001.

[42] V. P. Plagianakos, G. D. Magoulas, and M. N. Vrahatis, "Supervised Training Using Global Search Methods," in *Advances in Convex Analysis and Global Optimization*, 2013, pp. 3–14.

[43] V. P. Plagianakos, D. G. Sotiropoulos, and M. N. Vrahatis, "An Improved BP method with adaptative lerarning," in *Advances in Convex Analysis and Global Optimization*, 2008, pp. 1–5.

[44] N. K. Treadgold and T. D. Gedeon, "Simulated annealing and weight decay in adaptive learning: The SARPROP algorithm," *IEEE Trans. Neural Networks*, vol. 9, no. 4, pp. 662–668, 1998.

[45] D. B. Fogel, L. J. Fogel, and V. W. Porto, "Evolving neural networks," *Biological Cybern.*, vol. 63, no. 6, pp. 487–493, 1990.

[46] S. Mirjalili, "How effective is the Grey Wolf optimizer in training multi-layer perceptrons," *Appl. Intell.*, vol. 43, no. 1, pp. 150–161, 2015.

[47] S. Mirjalili, S. Mohammad, and A. Lewis, "Advances in Engineering Software Grey Wolf Optimizer," *Adv. Eng. Softw.*, vol. 69, pp. 46–61, 2014.

[48] Y. Tonce, K. Priyanto, and A. P. System, "Multi Objective Optimal Power Flow To Minimize Losses and Carbon Emission Using Wolf Algorithm," in *International Seminar on Intelligent Technology and Its Applications*, 2015, pp. 153–158.

[49] Y. Chen, G. Zhang, T. Jin, S. Wu, and B. Peng, "Quantitative modelling of electricity consumption using computational intelligence aided design," *J. Clean. Prod.*, vol. 69, pp. 143–152, 2014.

[50] N. Singh-miller, M. Collins, and T. J. Hazen, “Dimensionality Reduction for Speech Recognition Using Neighborhood Components Analysis,” 2006.

[51] N. Kamarudin, S. A. R. Al-Haddad, S. J. Hashim, M. A. Nematollahi, and A. R. Bin Hassan, “Feature extraction using Spectral Centroid and Mel Frequency Cepstral Coefficient for Quranic Accent Automatic Identification,” in *2014 IEEE Student Conference on Research and Development, SCOReD 2014*, 2014, pp. 0–5.

[52] M. García, J. Poza, D. Abásolo, D. Santamarta, and R. Hornero, “Analysis of intracranial pressure signals recorded during infusion studies using the spectral entropy,” in *Conference proceedings :Annual International Conference of the IEEE Engineering in Medicine and Biology Society. IEEE Engineering in Medicine and Biology Society. Annual Conference*, 2013, vol. 2013, pp. 2543–2546.

[53] L. K. Isaacson, “Spectral entropy, empirical entropy and empirical exergy for deterministic boundary-layer structures,” *Entropy*, vol. 15, no. 10, pp. 4134–4158, 2013.

[54] A. M. Toh, R. Togneri, and S. Nordholm, “Spectral entropy as speech features for speech recognition,” *Comput. Eng.*, no. 1, pp. 22–25, 2005.

[55] Y. Yan, S. Member, L. Xu, S. Member, and P. Lee, “Mass Flow Measurement of Fine Particles in a Pneumatic Suspension Using Electrostatic Sensing and Neural Network Techniques,” *IEEE Trans. Instrum. Meas.*, vol. 55, no. 6, pp. 2330–2334, 2006.

[56] M. Nait Amar, N. Zeraibi, and K. Redouane, “Bottom hole pressure estimation using hybridization neural networks and grey wolves optimization,” *Petroleum*, vol. 4, no. 4, pp. 419–429, 2018.